

 Open access • Journal Article • DOI:10.1002/MP.14368

Repeatability of radiomic features in magnetic resonance imaging of glioblastoma: Test—retest and image registration analyses — [Source link](#)

Isaac Shiri, [Ghasem Hajianfar](#), [Ahmad Sohrabi](#), [Hamid Abdollahi](#) ...+7 more authors

Institutions: [Geneva College](#), [Iran University of Medical Sciences](#), [Tehran University of Medical Sciences](#), [University of British Columbia](#) ...+1 more institutions

Published on: 01 Sep 2020 - [Medical Physics](#) (Wiley)

Topics: [Image registration](#), [Image processing](#), [Standard test image](#) and [Image segmentation](#)

Related papers:

- [The Image Biomarker Standardization Initiative: Standardized Quantitative Radiomics for High-Throughput Image-based Phenotyping](#)
- [Computational Radiomics System to Decode the Radiographic Phenotype](#)
- [Noninvasive Fuhrman grading of clear cell renal cell carcinoma using computed tomography radiomic features and machine learning](#)
- [Cardiac SPECT radiomic features repeatability and reproducibility: A multi-scanner phantom study](#)
- [Radiomics-based machine learning model to predict risk of death within 5-years in clear cell renal cell carcinoma patients](#)

Share this paper:    

View more about this paper here: <https://typeset.io/papers/repeatability-of-radiomic-features-in-magnetic-resonance-40vv0h3h2g>

**Repeatability of radiomic features in magnetic resonance imaging of glioblastoma
Test–retest and image registration analyses**

Shiri, Isaac; Hajianfar, Ghasem; Sohrabi, Ahmad; Abdollahi, Hamid; P. Shayesteh, Sajad;
Geramifar, Parham; Zaidi, Habib; Oveisi, Mehrdad; Rahmim, Arman

Published in:
Medical Physics

DOI:
10.1002/mp.14368

Publication date:
2020

Document version:
Accepted manuscript

Citation for published version (APA):

Shiri, I., Hajianfar, G., Sohrabi, A., Abdollahi, H., P. Shayesteh, S., Geramifar, P., Zaidi, H., Oveisi, M., & Rahmim, A. (2020). Repeatability of radiomic features in magnetic resonance imaging of glioblastoma: Test–retest and image registration analyses. *Medical Physics*, 47(9), 4265-4280. <https://doi.org/10.1002/mp.14368>

Go to publication entry in University of Southern Denmark's Research Portal

Terms of use

This work is brought to you by the University of Southern Denmark.
Unless otherwise specified it has been shared according to the terms for self-archiving.
If no other license is stated, these terms apply:

- You may download this work for personal use only.
- You may not further distribute the material or use it for any profit-making activity or commercial gain
- You may freely distribute the URL identifying this open access version

If you believe that this document breaches copyright please contact us providing details and we will investigate your claim.
Please direct all enquiries to puresupport@bib.sdu.dk

1 Repeatability of Radiomic Features in Magnetic Resonance 2 Imaging of Glioblastoma: Test-Retest and Image Registration 3 Analyses

4
5 Isaac Shiri¹, Ghasem Hajianfar², Ahmad Sohrabi³, Hamid Abdollahi⁴, Sajad P. Shayesteh⁵,
6 Parham Geramifar⁶, Habib Zaidi^{1,7,8,9}, Mehrdad Oveisi^{2,10}, Arman Rahmim^{11,12}

- 7 1. Division of Nuclear Medicine and Molecular Imaging, Geneva University Hospital, CH-1211
8 Geneva 4, Switzerland
- 9 2. Rajaie Cardiovascular Medical and Research Center, Iran University of Medical Science,
10 Tehran, Iran
- 11 3. Cancer Control Research Center, Cancer Control Foundation, Iran University of medical
12 sciences, Tehran, Iran
- 13 4. Department of Radiologic Sciences and Medical Physics, Faculty of Allied Medicine, Kerman
14 University of Medical Science, Kerman, Iran
- 15 5. Department of Physiology, Pharmacology and Medical Physics, Faculty of Medicine, Alborz
16 University of Medical Sciences, Karaj, Iran
- 17 6. Research Center for Nuclear Medicine, Shariati Hospital, Tehran University of Medical
18 Sciences, Tehran, Iran
- 19 7. Geneva University Neurocenter, Geneva University, Geneva, Switzerland
- 20 8. Department of Nuclear Medicine and Molecular Imaging, University of Groningen, University
21 Medical Center Groningen, Groningen, Netherlands
- 22 9. Department of Nuclear Medicine, University of Southern Denmark, Odense, Denmark
- 23 10. Department of Computer Science, University of British Columbia, Vancouver BC, Canada
- 24 11. Departments of Radiology and Physics, University of British Columbia, Vancouver BC,
25 Canada
- 26 12. Department of Integrative Oncology, BC Cancer Research Centre, Vancouver BC, Canada

27 28 **Corresponding Author:**

29 Arman Rahmim, PhD, DABSNM

30 Associate Professor of Radiology and Physics, University of British Columbia

This is the author manuscript accepted for publication and has undergone full peer review but has not been through the copyediting, typesetting, pagination and proofreading process, which may lead to differences between this version and the [Version of Record](#). Please cite this article as [doi: 10.1002/MP.14368](https://doi.org/10.1002/MP.14368)

This article is protected by copyright. All rights reserved

31 Senior Scientist & Provincial Medical Imaging Physicist, BC Cancer Agency
32 BC Cancer Research Center
33 675 West 10th Ave
34 Office 6-112
35 Vancouver, BC, V5Z 1L3
36 Phone: 604-675-8262
37 Email: arman.rahmin@ubc.ca

38
39
40 **Short Running Title:** Repeatability of MRI Radiomic Features

41 **ABSTRACT**

42 **Purpose:** To assess repeatability of radiomic features in magnetic resonance (MR) imaging of
43 glioblastoma (GBM) tumors with respect to test-retest, different image registration approaches
44 and inhomogeneity bias field correction.

45 **Methods:** We analyzed MR images of 17 GBM patients including T1 and T2-weighted images
46 (performed within the same imaging unit on two consecutive days). For image segmentation,
47 we used a comprehensive segmentation approach including entire tumor, active area of tumor,
48 necrotic regions in T1-weighted images, and edema regions in T2-weighted images (test studies
49 only; registration to retest studies is discussed next). Analysis included N3, N4 as well as no
50 bias correction performed on raw MR images. We evaluated 20 image registration approaches,
51 generated by cross-combination of 4 transformation and 5 cost function methods. In total, 714
52 images (17 patients \times 2 images \times ((4 transformations \times 5 cost functions) + 1 test image) and
53 2856 segmentations (714 images \times 4 segmentations) were prepared for feature extraction.
54 Various radiomic features were extracted, including the use of pre-processing filters,
55 specifically wavelet (WAV) and Laplacian of Gaussian (LOG), as well as discretizations into
56 fixed bin width and fixed bin count (16, 32, 64, 128 and 256), Exponential, Gradient,
57 Logarithm, Square and Square Root scales. Intra-class correlation coefficients (ICC) were
58 calculated to assess repeatability of MRI radiomic features (high repeatability defined as ICC
59 $\geq 95\%$).

60 **Results:** In our ICC results, we observed high repeatability (ICC $\geq 95\%$) with respect to image
61 preprocessing, different image registration algorithms and test-retest analysis, for: RLNU and
62 GLNU from GLRLM, GLNU and DNU from GLDM, Coarseness and Busyness from
63 NGTDM, GLNU and ZP from GLSZM, and Energy and RMS from first order. Highest fraction
64 (percent) of repeatable features were observed, amongst registration techniques, for the method
65 Full Affine transformation with 12 degrees of freedom using Mutual Information cost function

66 (mean 32.4%), and amongst image processing methods, for the method Laplacian of Gaussian
67 (LOG) with Sigma (2.5-4.5 mm) (mean 78.9%). The trends were relatively consistent for N4,
68 N3 or no bias correction.

69 **Conclusion:** Our results showed varying performances in repeatability of MR radiomic
70 features for GBM tumors due to test-retest and image registration. The findings have
71 implications for appropriate usage in diagnostic and predictive models.

72 **Keywords:** Radiomics, MRI, Test–retest, Repeatability, Glioblastoma, Image registration, bias
73 correction.**INTRODUCTION**

74 Glioblastoma multiform (GBM) is a very heterogeneous cancer with poor prognosis and
75 treatment outcome ¹. The median survival for GBM patients is about 15 months and its
76 occurrence rate is two or three cases per 100,000 per year ². Surgical resection followed by
77 radiotherapy and chemotherapy is the current standard approach to treat GBM ³. In this context,
78 magnetic resonance imaging (MRI) plays a critical role in clinical diagnosis and treatment,
79 particularly towards informed surgery and radiotherapy treatment planning ³.

80 For years, qualitative MR image sequences have been used for GBM management. In recent
81 years, quantitative image-derived so-called radiomic features extracted from standard MR
82 images have been increasingly studied as powerful prognostic tools to enhance patient
83 management through improved stratification ⁴. Studies have identified that MR image features
84 extracted from GBM tumors are highly correlated with tumor heterogeneity, response failure
85 and survival⁵⁻⁷, metastasis and genomic parameters⁸⁻¹¹ (as reviewed in ¹²).

86 Radiomics is an active area of research, aiming to quantify images using different feature
87 categories towards improved clinical tasks ¹³⁻¹⁷. In radiomics studies, a wide range of features
88 are extracted from high quality images for several applications, such as clinical correlations,
89 therapy response prediction, tumor characterization and survival assessment ¹⁸⁻²¹. Radiomics is
90 a multi-step process applied to medical images involving image segmentation, feature
91 extraction, feature selection and multivariate analysis^{21,22}. Variations in these main steps and
92 their sub-steps, may result in notable alterations in radiomic features as considered for final
93 outcome analysis. Although radiomic analyses are becoming increasingly mature, there are a
94 number of important technical limitations, and many radiomic features are vulnerable to
95 significant variations based on image acquisition, reconstruction and processing methods, as
96 reported by ongoing radiomics studies ²³⁻²⁷. Moreover, as hundreds of feature sets are available
97 for consideration in medical imaging, it is necessary to consider the reproducibility and
98 repeatability of radiomic features as a feasible measure to pre-select features for further
99 analysis, such as classification and clinical correlation ²³.

100 In image biomarkers development, there are two main frontiers which should be assessed in
101 regard to robustness of radiomic features. Specifically, repeatability and reproducibility of
102 radiomic features can be important towards discovery of high-performance image biomarkers
103 for using in preclinical or clinical settings. The Quantitative Imaging Biomarker Alliance
104 (QIBA) Technical Performance Working Group has defined repeatability as the “variability of
105 the image biomarker when repeated measurements are acquired on the same experimental unit
106 under identical or nearly identical conditions” and reproducibility as “the variability in the
107 image biomarker measurements associated with using the imaging instrument in real world
108 clinical settings which are subject to a variety of external factors that cannot all be tightly
109 controlled”²⁸.

110 Although a number of studies have been conducted on repeatability and reproducibility of
111 radiomic features in different imaging modalities, some issues remain to be explored,
112 particularly for MRI radiomic features in GBM cancer^{29,30}. Gourtsoyianni *et al.*³¹ assessed
113 day-to-day repeatability of global and local regional MR imaging texture features derived from
114 primary rectal cancer, and demonstrated that repeatability is higher for global texture
115 parameters relative to local-regional texture parameters, indicating that global texture
116 parameters should be sufficiently robust for clinical practice. Baessler *et al.*³² investigated the
117 robustness of radiomic features in different MRI sequences. In that study, a phantom was
118 scanned on a clinical 3T system using FLAIR, T1w, and T2w sequences, and scans were
119 repeated after repositioning of the phantom. The study showed that only 15 of 45 features had
120 good robustness across all MRI sequences. Including repeatable features in diagnostic and
121 predictive models can be key for ensuring model generalizability³³⁻³⁵. As such, the present
122 study focuses on the study of repeatability, but in a novel context of studying image registration
123 methods for mapping retest images to test images. As image registration plays a critical role in
124 several clinical settings, such as treatment planning, we studied the temporal variations of MR
125 imaging features in two consecutive days.

134
135
136
137
138
139
140
141
142
143
144
145
146
147
148
149
150
151
152
153
154
155
156
157
158
159
160
161
162
163
164
165
166
167

MATERIAL AND METHODS

Figure 1 illustrates the various processes followed in this work, as elaborated below. Repeatability assesses feature variability in the context of varying imaging times (test-retest) under otherwise similar processes.

Patient data

We included 19 patients with pathologically confirmed GBM. The RIDER NEURO MRI ³⁶ dataset were obtained from the cancer imaging archive (TCIA) ^{36,37} were used for this study. All patients had two MR images, including T1- (gradient echo (GRE), gadolinium enhanced) and T2- (fluid attenuation inversion recovery (FLAIR), gadolinium enhanced) weighted sequences which had been acquired in two consequent days with the same protocols on a 1.5 tesla MRI scanner (Siemens Healthcare, SYNGO MR 2004V 4VB11D). Image acquisition and reconstruction parameter details were presented in Table 1. After reviewing all images, two patients were excluded: one patient because of challenges on finding the tumor, and another patient because of missing second day images. Finally, we analyzed MR images of 17 (two patients were excluded from 19 patients because of low image quality and miss one the image sequence) GBM patients including T1 and T2-weighted images.

Image segmentation

We performed all image segmentations manually using the open source software ITK-Snap ³⁸. For image segmentation, we used a comprehensive segmentation approach based on BRATS^{39,40} including a) entire tumor (enhancing + necrotic core), b) active area of tumor (enhancing core), c) necrotic regions (necrotic core) in T1-weighted images, and d) edema regions (edema core) in T2-weighted images (test studies only; registration to retest studies is discussed next). In total, the following segmentations were obtained per patient: 3 segmentations in the T1 weighted image, and 1 segmentation in the T2 weighted image. This was followed by reciprocal transfer of segmentations from T1 (T2) to T2 (T1) weighted images, arriving at 8 segmentations in total (4 on T1 and 4 on T2) for each patient.

168 **Image registration**

169 Each segmentation performed above for a given patient image was naturally mapped to the
170 subsequent follow-up image following image registration of retest images to test images.
171 Overall, we performed 20 types of image registrations obtained by cross combination of 4
172 transformations and 5 cost function methods, using Mango open source software ⁴¹. For
173 transformation, we applied full affine (FA), full scale (FS), global scale (GS) and rigid-body
174 (RB) with 12, 9, 7 and 6 degrees of freedom (DOF), respectively. Cost functions consisted of
175 correlation ratio (CR), mutual information (MI), normalized mutual information (NMI),
176 normalized correlation (NC) and least squares (LS).

177 **Feature extraction**

178 In total, 714 images (17 patients \times 2 images \times ((4 transformations \times 5 cost functions) + 1 test
179 image))) and 2856 segmentations (714 images \times 4 segmentations) were prepared for feature
180 extraction. The N3⁴² and N4⁴³ bias correction methods were additionally applied on raw MRI
181 images. For pre-processing, we applied filters including wavelet (all possible combinations of
182 applying either a high or a low pass filter in each of the three dimensions, including HHH,
183 HHL, HLH, HLL, LHH, LHL, LLH and LLL)) and Laplacian of Gaussian (LOG) with
184 different sigma values (0.5 to 5 with steps 0.5) all with 64 bins. Subsequently, images were
185 discretized into 16, 32, 64, 128 and 256 fixed bin count and fixed bin widths, Exponential,
186 Gradient, Logarithm, Square and Square Root scales. Three types of features, namely first-
187 order, shape-based and textural features, were then extracted. Texture sets consisted of gray
188 level co-occurrence matrix (GLCM), gray level run length matrix (GLRLM), gray level
189 dependence matrix (GLDM), gray level size zone matrix (GLSZM) and neighboring gray tone
190 difference matrix (NGTDM). In sum, more than twenty-six million (26,295,192) features were
191 extracted from the original as well as N3 and N4 bias corrected images for further analysis.
192 Details on image features are shown in Supplementary Table 1. Different tools have been
193 developed for extraction of radiomics feature ⁴⁴⁻⁴⁷. Our current study performs mage feature
194 extraction using the Python library PyRadiomics ⁴⁴ which the feature definition is compliant
195 with the Image biomarker standardization initiative (IBSI) . As an exception, the definition of
196 Kurtosis from first order features differs between PyRadiomics and IBSI. IBSI and
197 PyRadiomics calculates Kurtosis with -3 and $+3$ respectively, and this stem from the fact that
198 a gaussian distribution has a kurtosis.

199 **Statistics and data analysis**

200 In the present work, we used applied intra-class correlation coefficient (ICC) test for analysis
201 of feature repeatability.

202 The intra-class correlation coefficient (ICC) is a widely used reliability index in test-retest,
203 interrater and interrater reliability analyses. ICC can be defined as follows:

$$204 \quad ICC = \frac{MS_R - MS_W}{MS_R + (k - 1)MS_W} \quad \text{Eq. 1}$$

205 where MS_R denotes mean square for rows (each feature value in test and retest), MS_W indicates
206 mean square for residual source of variance, k is the number of observers involved, and n is
207 the number of subjects.

208 Based on ICC, robust features were categorized into five categories, namely 1) $ICC < 50\%$,
209 2) $50\% < ICC < 80\%$, 3) $80\% < ICC < 90\%$, 4) $90\% < ICC < 95\%$ and 5) $ICC > 95\%$. Features
210 with $ICC > 95\%$ were defined as highly robust features. For comparison of image registration
211 methods, we reported the peak value of the probability density function for each feature set.
212 The R package, version 3.1.3 IRR, was used for ICC computations.

213 ICC results are shown by the probability density distribution (PDD), which is used to
214 provide quantitative statistical description of ICC. In PDD, shape, and peak value can be used
215 to compare the ICC results. Specifically, in our work, we use this framework to assess how
216 radiomic features are impacted against different image registration methods in the test-retest
217 setting.

218
219
220
221
222
223
224
225
226
227
228
229
230
231
232
233

234
235
236
237
238
239
240
241
242
243
244
245
246
247
248
249
250
251
252
253
254
255
256
257
258
259
260
261
262
263
264
265
266
267

RESULTS

Analyzing the large set of radiomic features obtained from image types, different bias corrections, image registrations, regions, as well as pre-processing and feature sets, here we report the most relevant findings, while other findings are presented as supplementary data.

Figure 2 illustrates ICC values (categorized 1 to 5: 1 = low and 5 = highly robust) of radiomic features as extracted from discretization with 64 gray level fixed bin width for different image registration algorithms (N4 bias corrected images). The ICC values for all shape features were found to be more than 95% due to the fact that same segmentations in test images were mapped onto retest images. As such, these features were excluded from further analysis. Several first-order (FO) features including RMS, Mean, TE, Energy and 90Percentile and RLNU from GLRLM had $ICC > 95\%$. In addition, for Laplacian of Gaussian (LOG) with Sigma (3.5 mm) and Wavelet with LLL decomposition preprocessing, as used prior to extraction of radiomic features (Figures 3 and 4 in N4 bias corrected images, respectively), the above-mentioned FO features were found to be robust. On the other hand, as shown in Figure 3, certain features including GLCM (CP, CT, IV, SS), GLDM (DNU, GLNU, GLV, SDE, SDHGLE), GLRLM (GLNU, GLV, RLNU), GLSZM (GLNU, SZNU, ZP), NGTDM (Busyness, Strength), were commonly robust to different image registration algorithms. Also, as shown in Figure 4, certain features including GLCM (DE), GLDM (DNU, GLNU), GLRLM (GLNU, RLNU), GLSZM (GLNU, ZP) were highly robust to different image registration algorithms. Supplemental Tables 2, 5 and 8 present the percent of each ICC group (for different image registration and image processing settings) for the original as well as N4 and N3 bias corrected images, respectively. Supplementary Tables 3 and 4 show the highest ($ICC > 95\%$) and lowest repeatable features ($ICC < 50\%$), respectively, for original images in different image processing and registration settings. Supplementary Tables 6 and 7 show these for N4 bias corrected images, while Supplementary Tables 9 and 10 show them for N3 bias corrected images. The other results for ICC values, including heat maps for fixed bin count (16, 32, 64, 128, 256), fixed bin width (16, 32, 128, 256), Exponential, Gradient, Logarithm, Square, Square Root, LOG and Wavelet are presented as supplementary Figures 1-17 and 18-33 and 33-50 for the original, N4 and N3 bias corrected images, respectively.

268
269
270
271
272
273
274
275
276
277
278
279
280
281
282
283
284
285
286
287
288
289
290
291
292
293
294
295
296
297
298
299
300
301

In Figure 5-a, we present bar plots depicting percent of five ICC categories for different image preprocessing methods (across all radiomic features and registration algorithms) in N4 bias corrected images. The results show LOG pre-processing with medium sigma (2.5-4.5 mm) with highest fraction (percent) of robust features (mean 78.9%). In addition, Figure 5-b depicts ICC bar plots of different registration methods (across all radiomic features and image preprocessing methods) for N4 bias corrected images. As shown, the FA method with MI cost function (mean 32.4%) vs. GS registration method with LS cost function (mean 18.8%) depicted highest vs. lowest fraction (percent) of robust features, respectively. Similar bar plots for Original and N3 Bias Corrected images are presented in supplementary Figures 75 and 77, respectively.

In Supplementary Figures 63-66, 67-70 and 71-74, we illustrate bar plots of ICC groups for radiomic features against applied registration algorithms for the original, N4 and N3 bias corrected images, respectively. Interestingly, it is seen that the reproducibility performances for each of these 3 sets of images (i.e. Original, N3 and N4) are relatively consistent with respect to one another. Specifically, Supplemental Figure 69 depicts LOG pre-processing filter in N4 Bias Corrected images, arriving at highest number of reproducible features amongst preprocessing methods. As also seen, FA method with MI cost function provided highest number of reproducible features (10.8-79.6% depending on LOG sigma value; optimized for 2.5-4.5mm), and GS method with LS methods depicted lowest (5.4-36.6%) number of reproducible features. Supplementary Figures 75 and 77 show ICC Bar plots for the original and N3 bias corrected images, respectively, for different image preprocessing methods (across all radiomics feature and registration algorithms), different registration methods (across all radiomic features and image preprocessing methods), and different features (across all radiomic features and image preprocessing methods), arriving at generally similar observations.

Supplementary Figure 76 show ICC bar plots of different features in N4 bias corrected images (different image preprocessing and registration algorithm). ICC results showed high repeatability for RLNU (90.8%) and GLNU (88.8%) from GLRLM, GLNU (76.1%) and DNU

302 (69.2%) from GLDM, Coarseness (65.8%) and Busyness (54.9%) from NGTDM, GLNU
303 (57.4%) and ZP (39.7%) from GLSZM, and Energy (65.5%) and RMS (64.9%) from first order
304 were most highly repeatable with respect to image preprocessing and different image
305 registration algorithms and test-retest analysis (ICC>95%). Correlation (24.4%) and AC
306 (22.7%) from GLCM, HGLZE (22.9%), LAE (22.6%) and ZV (22.5%) from GLSZM, HGLRE
307 (22.7%) from GLRLM, and HGLE from GLDM (22.7%) had lowest reproducibility with
308 respect to image preprocessing, different image registration algorithms and test-retest analysis
309 (with ICC<50%).

310 Figure 6-a shows ICC bar plots between Original and N3 bias corrected images (across all
311 radiomic features and registration algorithms). All preprocessed images except Fixed Bin
312 Width (FBW) had high reproducibility. Figure 6-b ICC shows bar plots between Original and
313 N4 bias corrected images (across all radiomic features and registration algorithms). It is
314 essentially seen that N4 bias correction alters images more significantly than N3, with respect
315 to Original images. Nonetheless, as discussed above, reproducibility performances within these
316 3 sets of images (Original, N3 and N4), are relative consistent with respect to one another.

317 Figure 7 (a-f) depicts the probability density of ICC distribution for different types of
318 radiomic features in N4 bias corrected images. The ICC distributions are different in several
319 aspects, including peak values, ICC distribution per image registration method and density
320 values. In Figure 7 (a-b), the main peak values of probability density for fixed bin count and
321 fixed bin width discretized radiomic features (64 bin discretization) are ≥ 5 , while in Figure 7
322 (c and d), the peak values of features (Square and Square Root) are ≥ 5 . For LOG features
323 (Figure 7 e), the peak values of probability density are more than 18, while for Wavelet
324 features, these values are more than 7.5. More details about the probability density plot are
325 presented in supplementary Figures 51-54, 55-58 and 59-62 for the original, N4 and N3 bias
326 corrected images, respectively.

327 Table 2 shows our results for highly repeatable features (ICC ≥ 0.95) against different
328 registration schemes for N4 bias corrected images (the highest value in each row is set to bold).
329 For all feature sets, highly repeatable features were found for the registration method FA-MI
330 (range; 17.2-32.3% for BIN, 10.8-79.6% for LOG & 6.45-45.2% for wavelet). For LOG
331 features, the highest repeatability was found for the RB-NMI registration scheme (82.8%).
332 More details on repeatability are provided in supplementary Tables 2, 5 and 8 for the original,
333 N4 and N3 bias corrected images, respectively. The results for features with ICC>95% and
334 ICC<50% against all registration methods are summarized in supplementary Tables 3-4,6-7
335 and 9-10 for original, N4 and N3 Bias corrected images, respectively. The number of high

336 reproducible features ($ICC > 95\%$) were 243, 358 and 268 for Original, N4 bias corrected and
337 N3 Bias corrected images, respectively (across all radiomic features, image preprocessing
338 methods and registration algorithms).

Author Manuscript

339 **DISCUSSION**

340 The assessment of repeatability and reproducibility for image features has garnered increasing
341 interest ²⁹. Accumulating evidence suggests the importance of taking such analyses into
342 account. Studies have emphasized that repeatable radiomic features must be used for predictive
343 modelling ³¹. In the present study, we aimed to assess test-retest repeatability of MRI radiomic
344 features in GBM cancer patients as well as their repeatability against a wide range of image
345 registration schemes. Different tools have been developed for radiomics feature extraction⁴⁴⁻⁴⁶;
346 our study was conducted using the PyRadiomics package according to consensus definitions
347 of the Image biomarker standardization initiative (IBSI) ^{48,49}. IBSI is an independent
348 international collaboration working towards standardization of image biomarkers. In this
349 approach, all image features are standardized in terms of definitions, image processing, and
350 reporting system.

351 In our ICC results, we observed high repeatability ($ICC \geq 95\%$) with respect to image
352 preprocessing, different image registration algorithms and test-retest analysis for: RLNU and
353 GLNU from GLRLM, GLNU and DNU from GLDM, Coarseness and Busyness from
354 NGTDM, GLNU and ZP from GLSZM, and Energy and RMS from first order features. In
355 addition, several first-order wavelet and LOG were found to be high-ICC features
356 (supplementary Figures 15-16). As comparison, Schwier *et al.* ⁵⁰ recently also reported that
357 first-order features Mean and Median had $ICC \geq 95\%$ in prostate MR image feature test-retest
358 analysis.

359 Image registration is a key consideration in treatment response evaluation and adaptive
360 radiotherapy. Our analysis shows that different image registration schemes have different
361 effects on radiomic features. Depending on registration settings including transformation and
362 cost function, feature performances vary. Highest percent of repeatable features were observed,
363 amongst registration methods for the method Full Affine with 12 degrees of freedom with
364 Mutual Information cost function (mean 78.9%), and amongst image processing methods for
365 the method Laplacian of Gaussian (LOG) with Sigma (2.5-4.5 mm) (mean 32.4%).

366 There are a number of feature robustness analysis studies indicating that radiomic feature
367 values vary with image acquisition and reconstruction parameters. Ford *et al.* ⁵¹ studied the
368 impact of pulse sequence parameter selection on MRI-based textural features of the brain. Pulse
369 sequences consisted of spin echo (SE), gradient echo (GRE), spoiled gradient echo (SP-GRE),
370 inversion recovery spin echo (IR-SE), and inversion recovery gradient echo (IR-GRE). They
371 found that radiomic features varied considerably among images generated by the five different
372 T1-weighted pulse sequences, and that deviations from those measured on the T1 map varied

373 among features, from a few percent to over 100%. Yang *et al.* ⁵² examined the dependence of
374 image texture features on MR acquisition parameters and reconstruction using a digital MR
375 imaging phantom. They studied the effects of varying levels of acquisition noise, three
376 acceleration factors, and four image reconstruction algorithms on MRI features. The
377 investigators observed feature variance due to reconstruction algorithm and acceleration factor
378 to be generally smaller than the clinical effect size. In that study, it was suggested that adequate
379 precautions need to be taken regarding the validity and reliability of texture features, although
380 some features had been preserved by changes in MR imaging settings. Molina *et al.* ⁵³ studied
381 potential variations of textural measures due to changes in MRI protocols including four
382 different spatial resolution combinations and three dynamic ranges. The results showed that no
383 textural measures were robust under dynamic range changes and entropy was the only textural
384 feature robust under spatial resolution changes. Imaging-based changes including acquisition
385 and reconstruction should be considered and separated from therapy related and tumor
386 biological changes. In our study, we observed that several radiomic features change
387 significantly across scan times.

388 Other researchers have attempted to assess robustness of radiomic features in different
389 imaging modalities including CT. Cunliffe *et al.* ⁵⁴ demonstrated that registration altered the
390 values of the majority of CT texture features. They applied their texture analysis on serial CT
391 scans and showed that 19 features remained relatively stable after demons registration,
392 indicating their potential for detecting pathologic change in serial CT scans. They also
393 indicated that combined use of accurate deformable registration using demons and texture
394 analysis may allow quantitative evaluation of local changes in lung tissue due to disease
395 progression or treatment response. Chou *et al.* ⁵⁵ evaluated radiomic features stability when
396 deformable image registration was applied. They applied feature analysis on lung cancer four-
397 dimensional computed tomography (4DCT), and deformable image registration (DIR) was
398 applied between the inspiration and expiration phases of 4DCT datasets. They concluded that
399 many features were unstable (mean variation > 50% or CCC < 0.5) when DIR is applied,
400 caution is needed in radiomic feature analysis when DIR is necessary.

401 A recent study performed by Lv *et al.* ⁵⁶ in nasopharyngeal PET/CT showed that some
402 radiomic features even with low ICC may perform well in disease discrimination. They
403 demonstrated that poor absolute scale reproducibility of radiomic features did not necessarily
404 translate into poor disease differentiation. In other words, features may change significantly
405 due to different kinds of processing, but their relative ordering may remain the same.
406 Nonetheless, this was a reproducibility study: in repeatability studies (including the present

407 work where for a given processing, test-retest values of features are evaluated), including high-
408 ICC repeatable radiomic features in diagnostic and predictive models may be critical for model
409 generalizability.

410 Low frequency intensity non-uniformity presence in MR images, defined as field bias, could
411 confound performance. To address this bias, different algorithms have been proposed including
412 N3⁴² and N4 bias correction⁵⁷. In the present study, we used N3 and N4 bias correction and
413 found that these algorithms had considerable impact on radiomic features. In reference to no
414 bias correction, N3 bias correction produced higher number of reproducible features compared
415 to the N4 algorithm, i.e. N3 algorithm had less impact on radiomics features with respect to
416 non-bias corrected images. In addition, we identified that LHL decomposition from wavelet
417 vs. exponential (as well as 64 fixed bin width) pre-processing led to highest vs. lowest number
418 of reproducible features, respectively.

419 Harmonization is also a critical issue in radiomics studies⁵⁸. Several studies have indicated
420 that image features have to be harmonized against parameters which have great impact on
421 feature values, such as scanner variations, reconstruction, imaging protocols⁵⁹⁻⁶¹. In our study,
422 all images were acquired on the same scanner using the same imaging protocol. As such, there
423 was no need to harmonize image features, yet studies are needed to test or investigate methods
424 to harmonize features in test-retest and registration methods. With regards to harmonization,
425 Hu *et al*⁶² demonstrated that normalized features have more stability⁶². In addition, Orhac *et*
426 *al*⁶⁰ showed that harmonization can be efficient at removing multicenter effects on textural
427 features.

428 Treatment response evaluation in GBM suffers from several uncertainties in differentiation
429 among pseudo-progression, pseudo-response, treatment related necrosis and true progression
430^{63,64}. Although, single imaging studies have found feasible results, several studies have
431 indicated that diagnosis of pseudo-progression could not be achieved by a single imaging
432 technique and suggested that serial imaging will results in improved diagnosis accuracy^{65,66}.
433 On the other hand, there are several variations in the clinical definitions of pseudo-progression
434 based on the imaging reports which requires higher-precision quantitative imaging⁶⁷. Some
435 radiomics studies have shown feasibility of MR image radiomic features to discriminate
436 between pseudo-progression compared to true progression⁶⁸⁻⁷⁰ and genomic mutation
437 prediction^{8-11,71,72} and treatment response assessments^{5,6}. In the present image biomarker
438 discovery era, our results would be important, wherein radiomic features with greatest
439 robustness to image registration between images may be more beneficial in clinical studies.
440 Specifically, because studies have suggested serial imaging for treatment response evaluation,

441 serial radiomic studies may benefit by integrating the identified robust radiomic features and
442 methods as candidate biomarkers for GBM response assessment and prediction.

443 The limitation of this work is mainly the number of patients. The results of this study should
444 be confirmed in a larger, multi-center dataset. In addition, the present work can be extended to
445 other types of MR images, including diffusion weighted and dynamic contrast enhanced, and
446 in other organs and diseases.

447

448 **CONCLUSION**

449 Repeatable radiomic features are potentially better candidates for usage in diagnostic and
450 predictive models. Our results showed varying performance in repeatability of MR radiomic
451 features for GBM tumors due to test-retest and image registration. The trends were relatively
452 consistent for N4, N3 or no bias correction. Full Affine with 12 degrees of freedom with Mutual
453 Information cost function and Laplacian of Gaussian (LOG) image processing resulted in
454 highest percent of repeatable features in image registration and image processing, respectively.

455

456

457 **Acknowledgments:** This work was supported by the BC Cancer Foundation and the Swiss
458 National Science Foundation under grant SNRF 320030_176052 and the Swiss Cancer
459 Research Foundation under Grant KFS-3855-02-2016.

460

461 **Conflict of Interest:** The authors have no relevant conflicts of interest to disclose.

462

463

464

465

466

467

468

469

470 **References**

- 471 1. Tran B, Rosenthal M. Survival comparison between glioblastoma multiforme and other
472 incurable cancers. *J Clin Neurosci.* 2010;17(4):417-421.
- 473 2. Hanif F, Muzaffar K, Perveen K, Malhi SM, Simjee SU. Glioblastoma multiforme: A review of its
474 epidemiology and pathogenesis through clinical presentation and treatment. *Asian Pac J*
475 *Cancer Prev: APJCP.* 2017;18(1):3.
- 476 3. Davis ME. Glioblastoma: overview of disease and treatment. *Clin J Oncol Nurs.* 2016;20(5):S2.
- 477 4. Aerts HJ. The potential of radiomic-based phenotyping in precision medicine: a review. *JAMA*
478 *oncology.* 2016;2(12):1636-1642.
- 479 5. Kickingereder P, Götz M, Muschelli J, et al. Large-scale radiomic profiling of recurrent
480 glioblastoma identifies an imaging predictor for stratifying anti-angiogenic treatment
481 response. *Clin Cancer Res.* 2016;22(23):5765-5771.
- 482 6. Prasanna P, Patel J, Partovi S, Madabhushi A, Tiwari P. Radiomic features from the peritumoral
483 brain parenchyma on treatment-naive multi-parametric MR imaging predict long versus short-
484 term survival in glioblastoma multiforme: preliminary findings. *Eur Radiol.* 2017;27(10):4188-
485 4197.
- 486 7. Kickingereder P, Burth S, Wick A, et al. Radiomic Profiling of Glioblastoma: Identifying an
487 Imaging Predictor of Patient Survival with Improved Performance over Established Clinical and
488 Radiologic Risk Models. *Radiology.* 2016;280(3):880-889.
- 489 8. Hajianfar G, Shiri I, Maleki H, et al. Noninvasive O6 Methylguanine-DNA Methyltransferase
490 Status Prediction in Glioblastoma Multiforme Cancer Using Magnetic Resonance Imaging
491 Radiomics Features: Univariate and Multivariate Radiogenomics Analysis. *World Neurosurg.*
492 2019;132:e140-e161.
- 493 9. Kickingereder P, Bonekamp D, Nowosielski M, et al. Radiogenomics of glioblastoma: machine
494 learning-based classification of molecular characteristics by using multiparametric and
495 multiregional MR imaging features. *Radiology.* 2016;281(3):907-918.
- 496 10. Nicolasjilwan M, Hu Y, Yan C, et al. Addition of MR imaging features and genetic biomarkers
497 strengthens glioblastoma survival prediction in TCGA patients. *J Neuroradiol.* 2015;42(4):212-
498 221.
- 499 11. Akbari H, Bakas S, Pisapia JM, et al. In vivo evaluation of EGFRvIII mutation in primary
500 glioblastoma patients via complex multiparametric MRI signature. *Neuro-oncology.*
501 2018;20(8):1068-1079.
- 502 12. Narang S, Lehrer M, Yang D, Lee J, Rao A. Radiomics in glioblastoma: current status, challenges
503 and potential opportunities. *Translational Cancer Research.* 2016;5(4):383-397.

- 504 13. Aerts HJWL, Velazquez ER, Leijenaar RTH, et al. Decoding tumour phenotype by noninvasive
505 imaging using a quantitative radiomics approach. *Nat Commun.* 2014;5:4006.
- 506 14. Lambin P, Rios-Velazquez E, Leijenaar R, et al. Radiomics: Extracting more information from
507 medical images using advanced feature analysis. *Eur J Cancer.* 2012;48(4):441-446.
- 508 15. Kumar V, Gu YH, Basu S, et al. Radiomics: the process and the challenges. *Magn Reson*
509 *Imaging.* 2012;30(9):1234-1248.
- 510 16. Abdollahi H, Mostafaei S, Cheraghi S, Shiri I, Mahdavi SR, Kazemnejad A. Cochlea CT radiomics
511 predicts chemoradiotherapy induced sensorineural hearing loss in head and neck cancer
512 patients: a machine learning and multi-variable modelling study. *Physica Medica.*
513 2018;45:192-197.
- 514 17. Rastegar S, Vaziri M, Qasempour Y, et al. Radiomics for classification of bone mineral loss: A
515 machine learning study. *Diagn Interv Imaging.* 2020;S2211-5684(20)30025-5.
- 516 18. Kotrotsou A, Zinn PO, Colen RR. Radiomics in brain tumors: an emerging technique for
517 characterization of tumor environment. *Magn Reson Imaging Clin N Am.* 2016;24(4):719-729.
- 518 19. Chaddad A, Zinn PO, Colen RR. Radiomics texture feature extraction for characterizing GBM
519 phenotypes using GLCM. Paper presented at: 2015 IEEE 12th International Symposium on
520 Biomedical Imaging (ISBI); 16-19 April 2015, 2015.
- 521 20. Nazari M, Shiri I, Hajianfar G, et al. Noninvasive Fuhrman grading of clear cell renal cell
522 carcinoma using computed tomography radiomic features and machine learning. *Radiol Med.*
523 2020;10.1007/s11547-020-01169-z.
- 524 21. Shiri I, Maleki H, Hajianfar G, et al. Next-Generation Radiogenomics Sequencing for Prediction
525 of EGFR and KRAS Mutation Status in NSCLC Patients Using Multimodal Imaging and Machine
526 Learning Algorithms. *Mol Imaging Biol.* 2020;10.1007/s11307-020-01487-8.
- 527 22. Mostafaei S, Abdollahi H, Kazempour Dehkordi S, et al. CT imaging markers to improve
528 radiation toxicity prediction in prostate cancer radiotherapy by stacking regression algorithm.
529 *Radiol Med.* 2020;125(1):87-97.
- 530 23. Lambin P, Leijenaar RT, Deist TM, et al. Radiomics: the bridge between medical imaging and
531 personalized medicine. *Nat Rev Clin Oncol.* 2017;14(12):749.
- 532 24. Hatt M, Tixier F, Pierce L, Kinahan PE, Le Rest CC, Visvikis D. Characterization of PET/CT images
533 using texture analysis: the past, the presenta... any future? *Eur J Nucl Med Mol I.*
534 2017;44(1):151-165.
- 535 25. Shiri I, Rahmim A, Ghaffarian P, Geramifar P, Abdollahi H, Bitarafan-Rajabi A. The impact of
536 image reconstruction settings on 18F-FDG PET radiomic features: multi-scanner phantom and
537 patient studies. *Eur Radiol.* 2017;27(11):4498-4509.

- 538 26. Abdollahi H, Shiri I, Heydari M. Medical Imaging Technologists in Radiomics Era: An Alice in
539 Wonderland Problem. *Iran J Public Health*. 2019;48(1):184.
- 540 27. Edalat-Javid M, Shiri I, Hajianfar G, et al. Cardiac SPECT radiomic features repeatability and
541 reproducibility: A multi-scanner phantom study. *Journal of Nuclear Cardiology*. J Nucl Cardiol.
542 2020;10.1007/s12350-020-02109-0
- 543 28. Raunig DL, McShane LM, Pennello G, et al. Quantitative imaging biomarkers: a review of
544 statistical methods for technical performance assessment. *Stat Methods Med Res*.
545 2015;24(1):27-67.
- 546 29. Traverso A, Wee L, Dekker A, Gillies R. Repeatability and Reproducibility of Radiomic Features:
547 A Systematic Review. *Int J Radiat Oncol Biol Phys*. 2018;102(4):1143-1158.
- 548 30. Shiri I, Abdollahi H, Shaysteh S, Mahdavi SR. Test-retest reproducibility and robustness
549 analysis of recurrent glioblastoma MRI radiomics texture features. *Iran J Radiol*. 2017. (5).
- 550 31. Gourtsoyianni S, Doumou G, Prezzi D, et al. Primary rectal cancer: repeatability of global and
551 local-regional MR imaging texture features. *Radiology*. 2017;284(2):552-561.
- 552 32. Baeßler B, Weiss K, Pinto DDSJr. Robustness and Reproducibility of Radiomics in Magnetic
553 Resonance Imaging: A Phantom Study. *Invest Radiol*. 2019;54(4):221-228.
- 554 33. Trattnig S. The Shift in Paradigm to Precision Medicine in Imaging: International Initiatives for
555 the Promotion of Imaging Biomarkers. In: Martí-Bonmatí L, Alberich-Bayarri A, eds. *Imaging*
556 *Biomarkers: Development and Clinical Integration*. Cham: Springer International Publishing;
557 2017:1-7.
- 558 34. Carot JM, Conchado A. Detecting Measurement Biases: Sources of Uncertainty, Accuracy, and
559 Precision of the Measurements. In: Martí-Bonmatí L, Alberich-Bayarri A, eds. *Imaging*
560 *Biomarkers: Development and Clinical Integration*. Cham: Springer International Publishing;
561 2017:101-113.
- 562 35. Martí-Bonmatí L, Alberich-Bayarri A. *Imaging biomarkers: development and clinical*
563 *integration*. Springer; 2016.
- 564 36. Barboriak D. Data From RIDER_NEURO_MRI. *The Cancer Imaging Archive*. 2015.
- 565 37. Clark K, Vendt B, Smith K, et al. The Cancer Imaging Archive (TCIA): maintaining and operating
566 a public information repository. *J Digit Imaging*. 2013;26(6):1045-1057.
- 567 38. Yushkevich PA, Piven J, Hazlett HC, et al. User-guided 3D active contour segmentation of
568 anatomical structures: significantly improved efficiency and reliability. *Neuroimage*.
569 2006;31(3):1116-1128.

- 570 39. Bakas S, Reyes M, Jakab A, et al. Identifying the best machine learning algorithms for brain
571 tumor segmentation, progression assessment, and overall survival prediction in the BRATS
572 challenge. *arXiv preprint arXiv:181102629*. 2018.
- 573 40. Menze BH, Jakab A, Bauer S, et al. *The Multimodal Brain Tumor Image Segmentation*
574 *Benchmark (BRATS)*. *IEEE Trans Med Imaging*. 2015;34(10):1993-2024
- 575 41. Lancaster JL, Cykowski MD, McKay DR, et al. Anatomical global spatial normalization.
576 *Neuroinformatics*. 2010;8(3):171-182.
- 577 42. Sled JG, Zijdenbos AP, Evans AC. A nonparametric method for automatic correction of
578 intensity nonuniformity in MRI data. *EEE Trans Med Imaging*. 1998;17(1):87-97.
- 579 43. Tustison NJ, Avants BB, Cook PA, et al. N4ITK: improved N3 bias correction. *EEE Trans Med*
580 *Imaging*. 2010;29(6):1310-1320.
- 581 44. Van Griethuysen JJ, Fedorov A, Parmar C, et al. Computational radiomics system to decode
582 the radiographic phenotype. *Cancer research*. 2017;77(21):e104-e107.
- 583 45. Nioche C, Orhac F, Boughdad S, et al. LIFEx: a freeware for radiomic feature calculation in
584 multimodality imaging to accelerate advances in the characterization of tumor heterogeneity.
585 *Cancer research*. 2018;78(16):4786-4789.
- 586 46. Davatzikos C, Rathore S, Bakas S, et al. Cancer imaging phenomics toolkit: quantitative imaging
587 analytics for precision diagnostics and predictive modeling of clinical outcome. *J Med Imaging*.
588 2018;5(1):011018.
- 589 47. Ashrafinia S. *Quantitative nuclear medicine imaging using advanced image reconstruction and*
590 *radiomics*, Johns Hopkins University; 2019.
- 591 48. Zwanenburg A, Vallières M, Abdalah MA, et al. The Image Biomarker Standardization
592 Initiative: standardized quantitative radiomics for high-throughput image-based phenotyping.
593 *Radiology*. 2020.191145.
- 594 49. Zwanenburg A, Leger S, Vallières M, Löck S. Image biomarker standardisation initiative. *arXiv*
595 *preprint arXiv:161207003*. 2016.
- 596 50. Schwier M, van Griethuysen J, Vangel MG, et al. Repeatability of Multiparametric Prostate
597 MRI Radiomics Features. *arXiv preprint arXiv:180706089*. 2018.
- 598 51. Ford J, Dogan N, Young L, Yang FJCM, imaging m. Quantitative radiomics: impact of pulse
599 sequence parameter selection on MRI-based textural features of the brain. *Contrast Media*
600 *Mol Imaging*. 2018;2018:1729071.
- 601 52. Yang F, Dogan N, Stoyanova R, Ford JCJPM. Evaluation of radiomic texture feature error due
602 to MRI acquisition and reconstruction: A simulation study utilizing ground truth. *Phys Med*.
603 2018;50:26-36.

- 604 53. Molina D, Pérez-Beteta J, Martínez-González A, et al. Influence of gray level and space
605 discretization on brain tumor heterogeneity measures obtained from magnetic resonance
606 images. *Comput Biol Med* 2016;78:49-57.
- 607 54. Cunliffe AR, Armato SG, Fei XM, Tuohy RE, Al-Hallaq HA. Lung texture in serial thoracic CT
608 scans: Registration-based methods to compare anatomically matched regions. *Med Phys*.
609 2013;40(6):061906.
- 610 55. Chou K-T, Latifi K, Moros EG, et al. Evaluation of Radiomic Features Stability When Deformable
611 Image Registration Is Applied. Paper presented at: BIOIMAGING2018.
- 612 56. Lv W, Yuan Q, Wang Q, et al. Robustness versus disease differentiation when varying
613 parameter settings in radiomics features: application to nasopharyngeal PET/CT. *Eur Radiol*.
614 2018;28(8):3245-3254.
- 615 57. Vovk U, Pernus F, Likar B. A review of methods for correction of intensity inhomogeneity in
616 MRI. *IEEE Trans Med Imaging*. 2007;26(3):405-421.
- 617 58. Yip SS, Aerts HJ. Applications and limitations of radiomics. *Phys Med Biol*.
618 2016;61(13):R150-R166.
- 619 59. Lasnon C, Majdoub M, Lavigne B, et al. 18 F-FDG PET/CT heterogeneity quantification through
620 textural features in the era of harmonisation programs: a focus on lung cancer. *Eur J Nucl Med*
621 *Mol Imaging*. 2016;43(13):2324-2335.
- 622 60. Orhac F, Boughdad S, Philippe C, et al. A post-reconstruction harmonization method for
623 multicenter radiomic studies in PET. *J Nucl Med*. 2018;59(8):1321-1328.
- 624 61. Chirra P, Leo P, Yim M, et al. Empirical evaluation of cross-site reproducibility in radiomic
625 features for characterizing prostate MRI. Paper presented at: Medical Imaging 2018:
626 Computer-Aided Diagnosis2018.
- 627 62. Hu P, Wang J, Zhong H, et al. Reproducibility with repeat CT in radiomics study for rectal
628 cancer. *Oncotarget*. 2016;7(44):71440.
- 629 63. Ellingson BM, Chung C, Pope WB, Boxerman JL, Kaufmann TJ. Pseudoprogression,
630 radionecrosis, inflammation or true tumor progression? Challenges associated with
631 glioblastoma response assessment in an evolving therapeutic landscape. *J Neurooncol*
632 2017;134(3):495-504.
- 633 64. Chu HH, Choi SH, Ryou I, et al. Differentiation of true progression from pseudoprogression in
634 glioblastoma treated with radiation therapy and concomitant temozolomide: comparison
635 study of standard and high-b-value diffusion-weighted imaging. *Radiology*. 2013;269(3):831-
636 840.

- 637 65. Thust SC, Van Den Bent MJ, Smits M. Pseudoprogession of brain tumors. *J Magn Reson*
638 *Imaging* 2018;48(3):571-589.
- 639 66. Brahm CG, Den Hollander MW, Enting RH, et al. Serial FLT PET imaging to discriminate
640 between true progression and pseudoprogession in patients with newly diagnosed
641 glioblastoma: a long-term follow-up study. *Eur J Nucl Med Mol Imaging* 2018;45(13):2404-
642 2412.
- 643 67. Zikou A, Sioka C, Alexiou GA, Fotopoulos A, Voulgaris S, Argyropoulou MI. Radiation necrosis,
644 pseudoprogession, pseudoresponse, and tumor recurrence: imaging challenges for the
645 evaluation of treated gliomas. *Contrast Media Mol Imaging*. 2018;2018.
- 646 68. Chaddad A, Kucharczyk MJ, Daniel P, et al. Radiomics in glioblastoma: current status and
647 challenges facing clinical implementation. *Front Oncol*. 2019;9.
- 648 69. Elshafeey N, Kotrotsou A, Hassan A, et al. Multicenter study demonstrates radiomic features
649 derived from magnetic resonance perfusion images identify pseudoprogession in
650 glioblastoma. *Nat Commun* 2019;10(1):1-9.
- 651 70. Tiwari P, Prasanna P, Rogers L, et al. Texture descriptors to distinguish radiation necrosis from
652 recurrent brain tumors on multi-parametric MRI. Paper presented at: Medical Imaging 2014:
653 Computer-Aided Diagnosis2014.
- 654 71. Binder ZA, Thorne AH, Bakas S, et al. Epidermal Growth Factor Receptor Extracellular Domain
655 Mutations in Glioblastoma Present Opportunities for Clinical Imaging and Therapeutic
656 Development. *Cancer Cell*. 2018;34(1):163-177.e167.
- 657 72. Beig N, Patel J, Prasanna P, et al. Radiogenomic analysis of hypoxia pathway is predictive of
658 overall survival in Glioblastoma. *Sci Rep*. 2018;8(1):7.

659

Table 1. Image acquisition and reconstruction parameter details.

Images	Magnet	TE, TR	Resolution	Flip Angle
Contrast-enhanced 3D FLASH	1.5 T	TR: 8.6 ms	256 x 256	20 degree
		TE: 4.1 ms	1mm isotropic	
T2-weighted 3D FLAIR	1.5 T	TR: 6000 ms	256 x 256	180 degree
		TE: 353 ms	1mm isotropic	
		TI: 2200 ms		

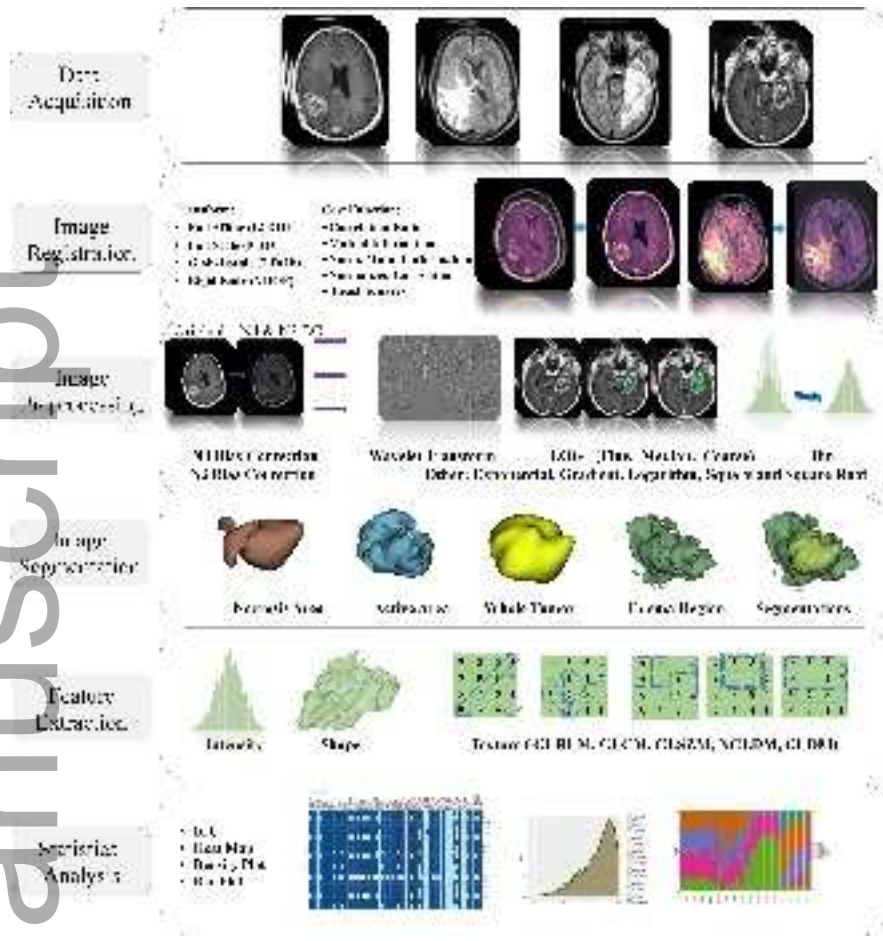
Author Manuscript

Registration	FA_CR	FS_CR	GS_CR	RB_CR	FA_LS	FS_LS	GS_LS	RB_LS	FA_MI	FS_MI	GS_MI	RB_MI	FA_NC	FS_NC	GS_NC	RB_NC	FA_NMI	FS_NMI	GS_NMI	RB_NMI
FBC (16)	21.5	14	10.8	14	14	14	9.68	15.1	26.9	19.4	11.8	15.1	14	14	10.8	14	19.4	18.3	14	18.3
FBC (32)	19.4	15.1	11.8	15.1	16.1	16.1	9.68	15.1	24.7	19.4	12.9	18.3	16.1	16.1	11.8	15.1	21.5	19.4	15.1	20.4
FBC (64)	21.5	16.1	12.9	12.9	15.1	15.1	9.68	14	25.8	19.4	14	15.1	17.2	15.1	12.9	16.1	20.4	21.5	16.1	19.4
FBC (128)	18.3	12.9	11.8	14	15.1	14	11.8	14	21.5	17.2	12.9	11.8	14	12.9	11.8	14	17.2	17.2	15.1	16.1
FBC (256)	23.7	20.4	11.8	19.4	18.3	19.4	11.8	20.4	28	20.4	12.9	14	19.4	20.4	11.8	20.4	21.5	20.4	15.1	19.4
FBW (16)	21.5	17.2	16.1	18.3	17.2	17.2	15.1	17.2	25.8	22.6	17.2	17.2	18.3	18.3	16.1	17.2	22.6	22.6	20.4	20.4
FBW (32)	21.5	16.1	16.1	17.2	16.1	16.1	15.1	16.1	23.7	20.4	17.2	17.2	17.2	17.2	16.1	17.2	20.4	20.4	19.4	18.3
FBW (64)	18.3	12.9	12.9	12.9	12.9	12.9	11.8	12.9	20.4	16.1	15.1	15.1	12.9	12.9	12.9	12.9	16.1	15.1	16.1	16.1
FBW (128)	15.1	9.68	9.68	9.68	9.68	9.68	8.6	9.68	17.2	12.9	10.8	11.8	9.68	9.68	9.68	9.68	12.9	12.9	12.9	11.8
FBW (256)	30.1	26.9	26.9	26.9	25.8	25.8	24.7	25.8	32.3	30.1	28	24.7	22.6	23.7	26.9	25.8	30.1	30.1	30.1	28
Exponential	3.23	3.23	1.08	1.08	1.08	2.15	0	2.15	4.3	4.3	0	1.08	3.23	2.15	1.08	2.15	4.3	4.3	0	2.15
Gradient	9.68	9.68	7.53	10.8	9.68	8.6	3.23	9.68	10.8	9.68	7.53	7.53	9.68	9.68	7.53	9.68	10.8	9.68	6.45	9.68
Logarithm	14	12.9	7.53	14	12.9	12.9	4.3	12.9	14	11.8	11.8	11.8	11.8	7.53	6.45	15.1	12.9	12.9	12.9	14
Square	19.4	10.8	8.6	8.6	9.68	7.53	1.08	6.45	24.7	17.2	9.68	7.53	10.8	10.8	8.6	8.6	17.2	14	9.68	14
Square Root	19.4	18.3	11.8	15.1	16.1	16.1	10.8	15.1	24.7	19.4	14	17.2	16.1	15.1	11.8	14	17.2	16.1	14	22.6
LOG (S=0.5mm)	8.6	9.68	4.3	9.68	9.68	9.68	5.38	9.68	10.8	10.8	4.3	7.53	8.6	8.6	4.3	8.6	9.68	9.68	5.38	9.68
LOG (S=1.0mm)	41.9	33.3	17.2	35.5	32.3	34.4	6.45	32.3	49.5	36.6	21.5	21.5	34.4	33.3	18.3	35.5	36.6	36.6	21.5	38.7
LOG (S=1.5mm)	60.2	50.5	30.1	47.3	51.6	49.5	14	48.4	62.4	53.8	31.2	41.9	50.5	51.6	30.1	50.5	54.8	53.8	33.3	54.8
LOG (S=2.0mm)	64.5	54.8	40.9	54.8	55.9	54.8	24.7	54.8	66.7	58.1	43	48.4	55.9	55.9	40.9	55.9	58.1	57	43	60.2
LOG (S=2.5mm)	72	67.7	53.8	67.7	68.8	66.7	28	66.7	74.2	72	55.9	63.4	68.8	67.7	53.8	67.7	69.9	72	55.9	71
LOG (S=3.0mm)	77.4	71	55.9	69.9	72	69.9	36.6	71	79.6	78.5	59.1	69.9	72	71	55.9	69.9	77.4	78.5	59.1	75.3
LOG (S=3.5mm)	72	69.9	51.6	69.9	74.2	73.1	32.3	68.8	73.1	77.4	57	67.7	74.2	68.8	51.6	69.9	77.4	76.3	57	76.3
LOG (S=4.0mm)	72	79.6	55.9	78.5	79.6	79.6	31.2	78.5	73.1	80.6	59.1	66.7	79.6	80.6	55.9	79.6	80.6	80.6	57	78.5
LOG (S=4.5mm)	72	80.6	50.5	79.6	80.6	82.8	31.2	78.5	77.4	82.8	51.6	68.8	79.6	81.7	49.5	81.7	82.8	82.8	51.6	80.6
LOG (S=5.0mm)	66.7	65.6	44.1	64.5	66.7	65.6	30.1	64.5	66.7	68.8	46.2	65.6	68.8	66.7	44.1	66.7	69.9	69.9	46.2	71
Wavelet (HHH)	7.53	7.53	4.3	7.53	7.53	7.53	4.3	6.45	6.45	7.53	3.23	6.45	7.53	7.53	4.3	7.53	7.53	7.53	3.23	5.38
Wavelet (HHL)	7.53	8.6	3.23	6.45	6.45	6.45	2.15	6.45	8.6	7.53	3.23	7.53	7.53	8.6	3.23	6.45	7.53	7.53	3.23	7.53
Wavelet (HLH)	7.53	8.6	5.38	8.6	7.53	8.6	5.38	8.6	8.6	8.6	5.38	8.6	7.53	8.6	5.38	8.6	8.6	8.6	5.38	8.6
Wavelet (HLL)	7.53	7.53	5.38	8.6	7.53	7.53	3.23	7.53	9.68	8.6	5.38	7.53	7.53	8.6	6.45	8.6	7.53	7.53	5.38	7.53
Wavelet (LHH)	10.8	9.68	5.38	8.6	9.68	9.68	5.38	8.6	9.68	8.6	5.38	8.6	9.68	9.68	6.45	8.6	8.6	8.6	5.38	8.6
Wavelet (LHL)	10.8	10.8	3.23	11.8	9.68	9.68	2.15	11.8	11.8	11.8	2.15	11.8	9.68	10.8	3.23	10.8	11.8	11.8	2.15	11.8
Wavelet (LLH)	9.68	7.53	4.3	8.6	8.6	8.6	3.23	7.53	9.68	8.6	3.23	9.68	6.45	7.53	3.23	8.6	7.53	8.6	4.3	7.53
Wavelet (LLL)	44.1	38.7	25.8	36.6	38.7	37.6	16.1	35.5	45.2	41.9	30.1	37.6	36.6	35.5	24.7	37.6	44.1	40.9	30.1	44.1

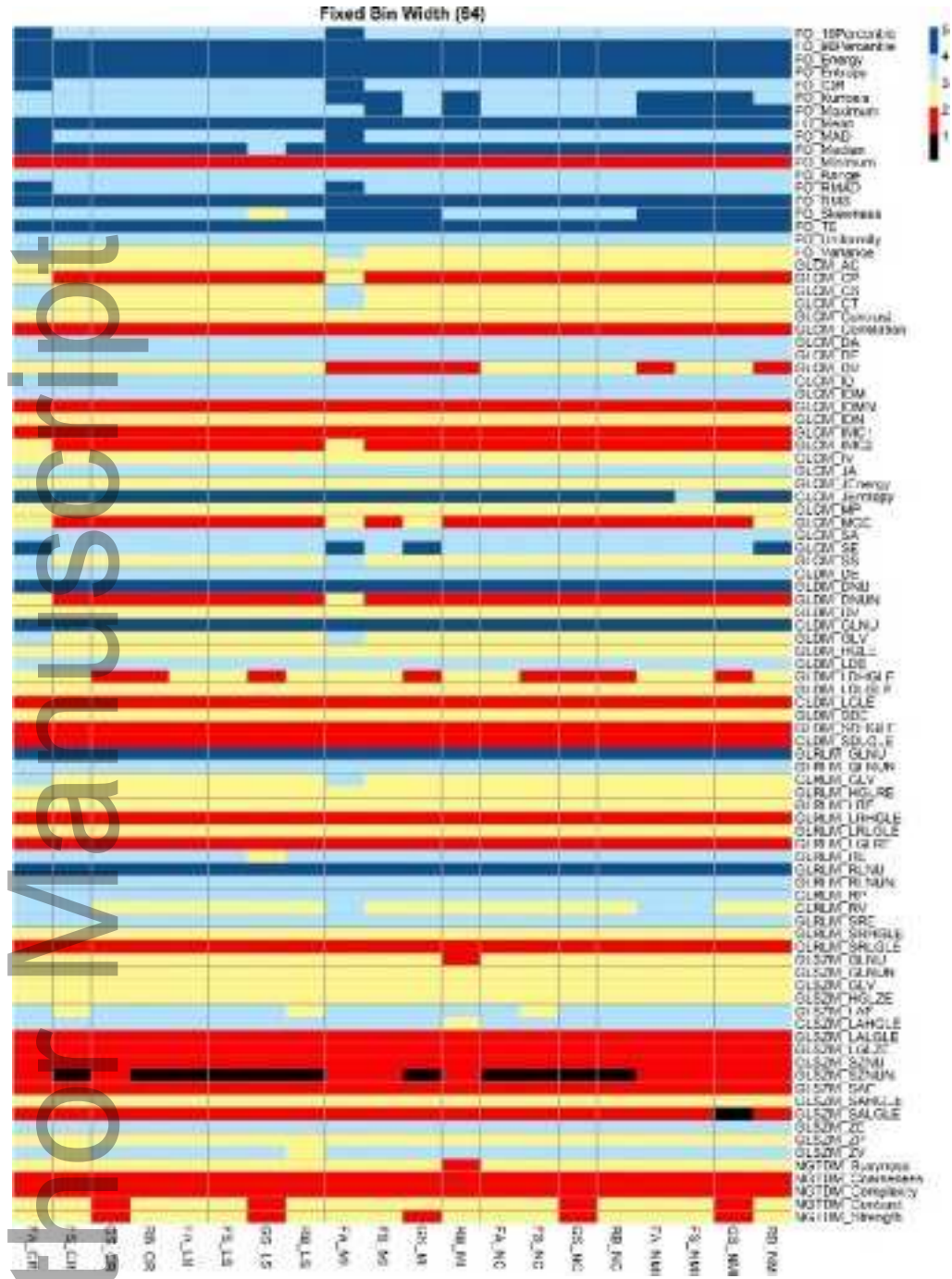
Table 2.
Highly repeatable features (ICC ≥ 0.95) against different registration settings in N4 bias corrected images.

Author Manuscript

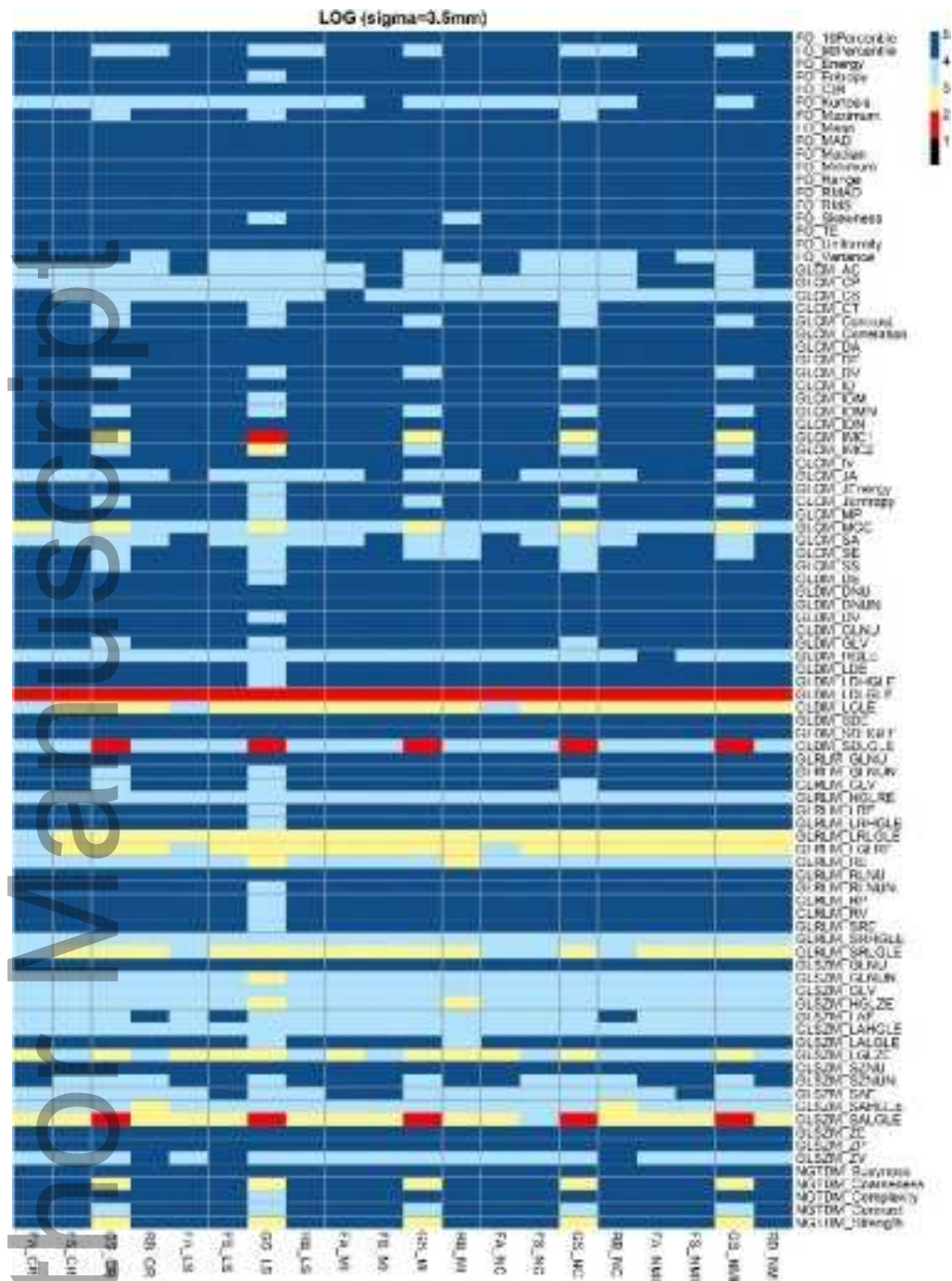
*FBC: Fixed Bin Count, FBW: Fixed Bin Width, LOG: Laplacian of Gaussian, S: Sigma



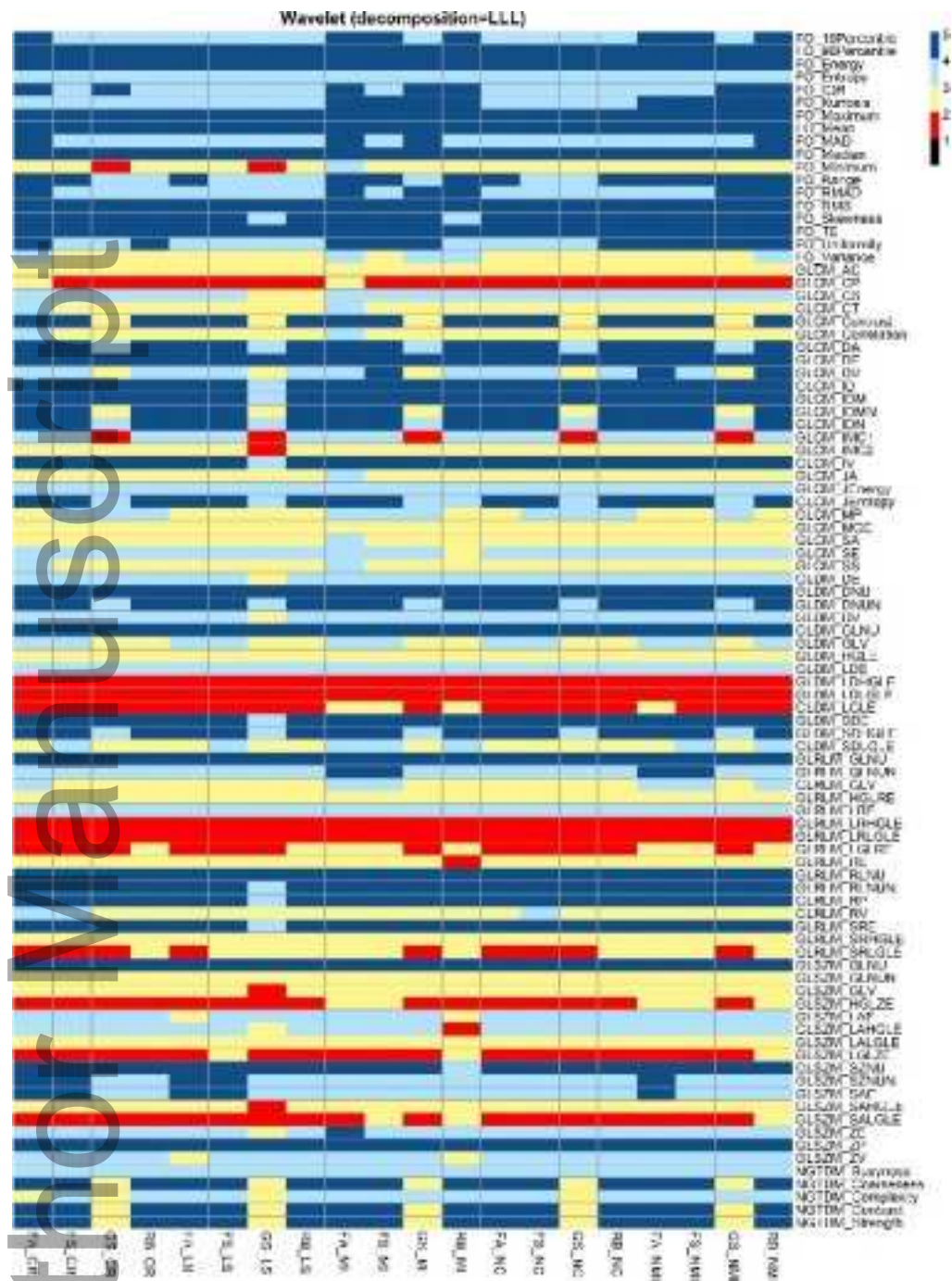
mp_14368_f1.jpg



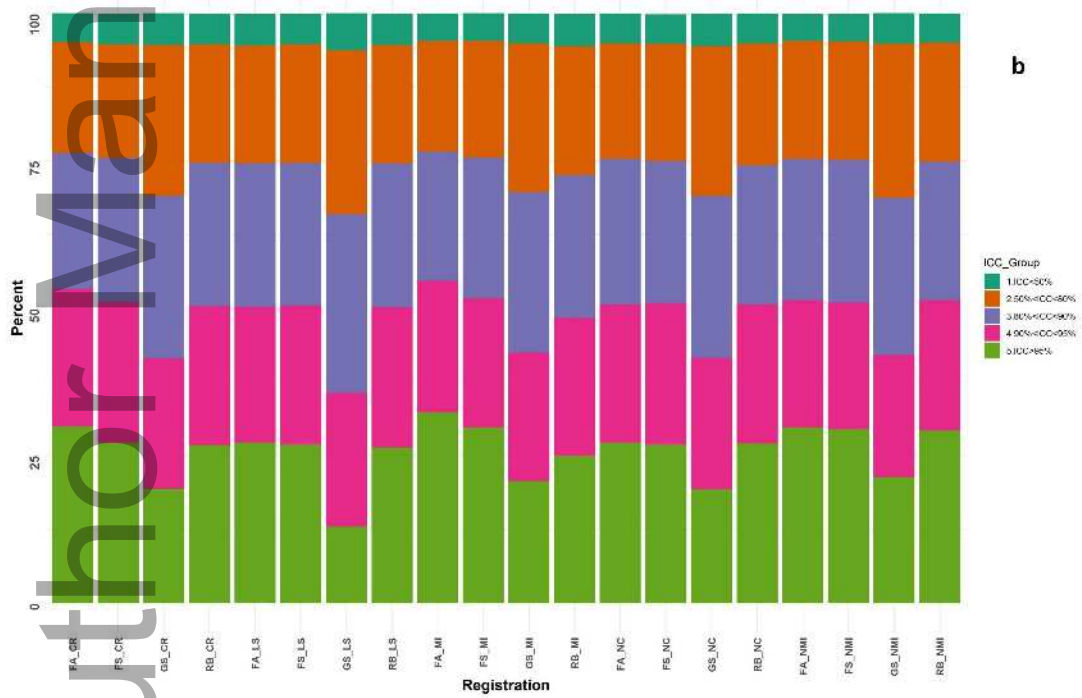
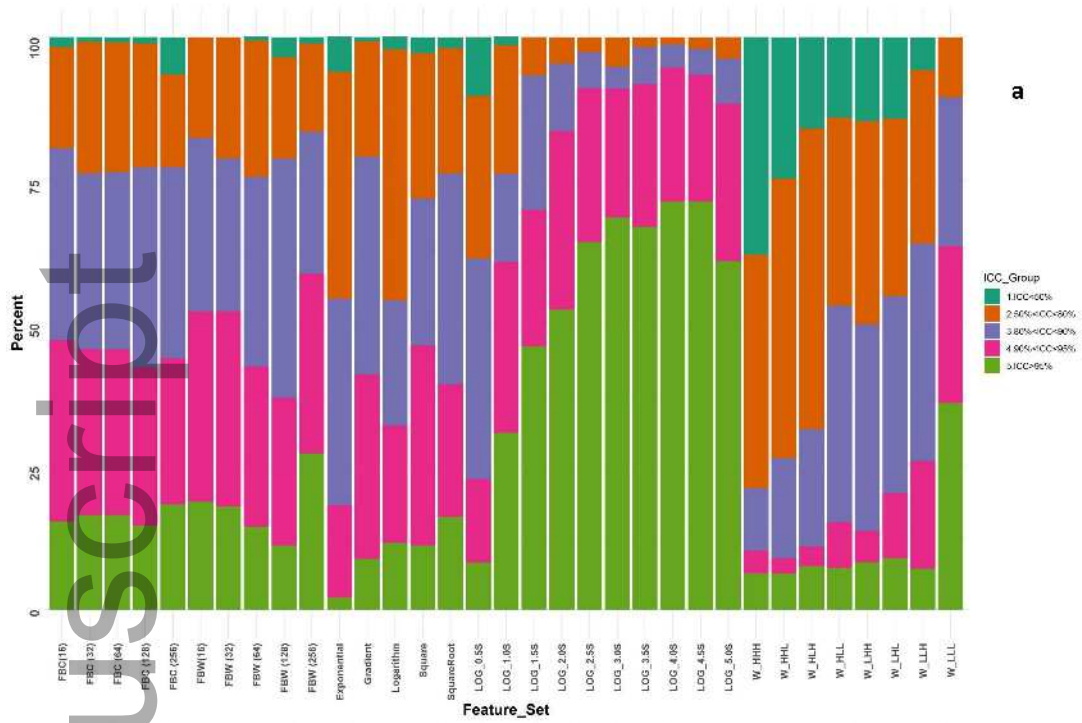
mp_14368_f2.jpg



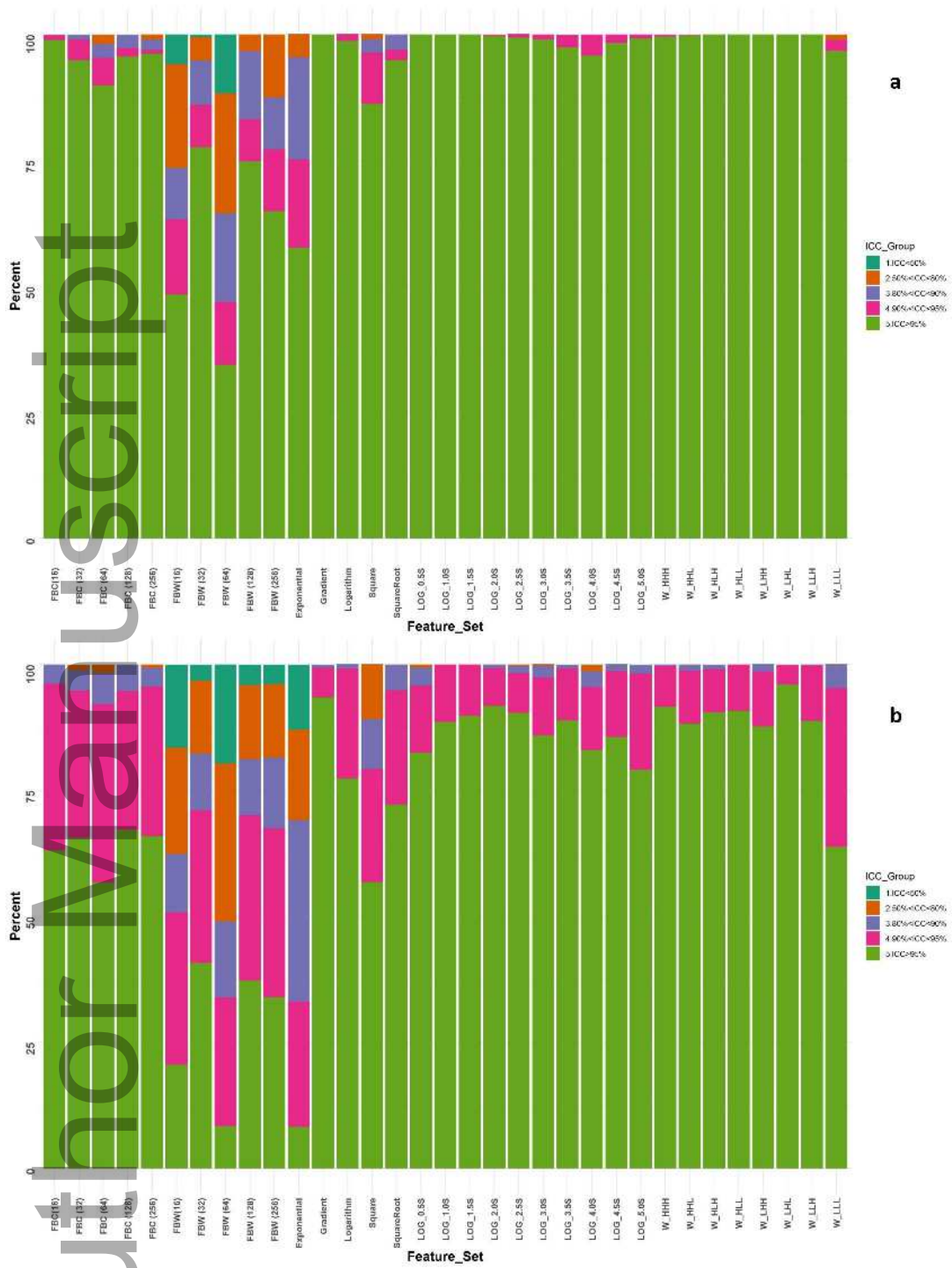
mp_14368_f3.jpg



mp_14368_f4.jpg

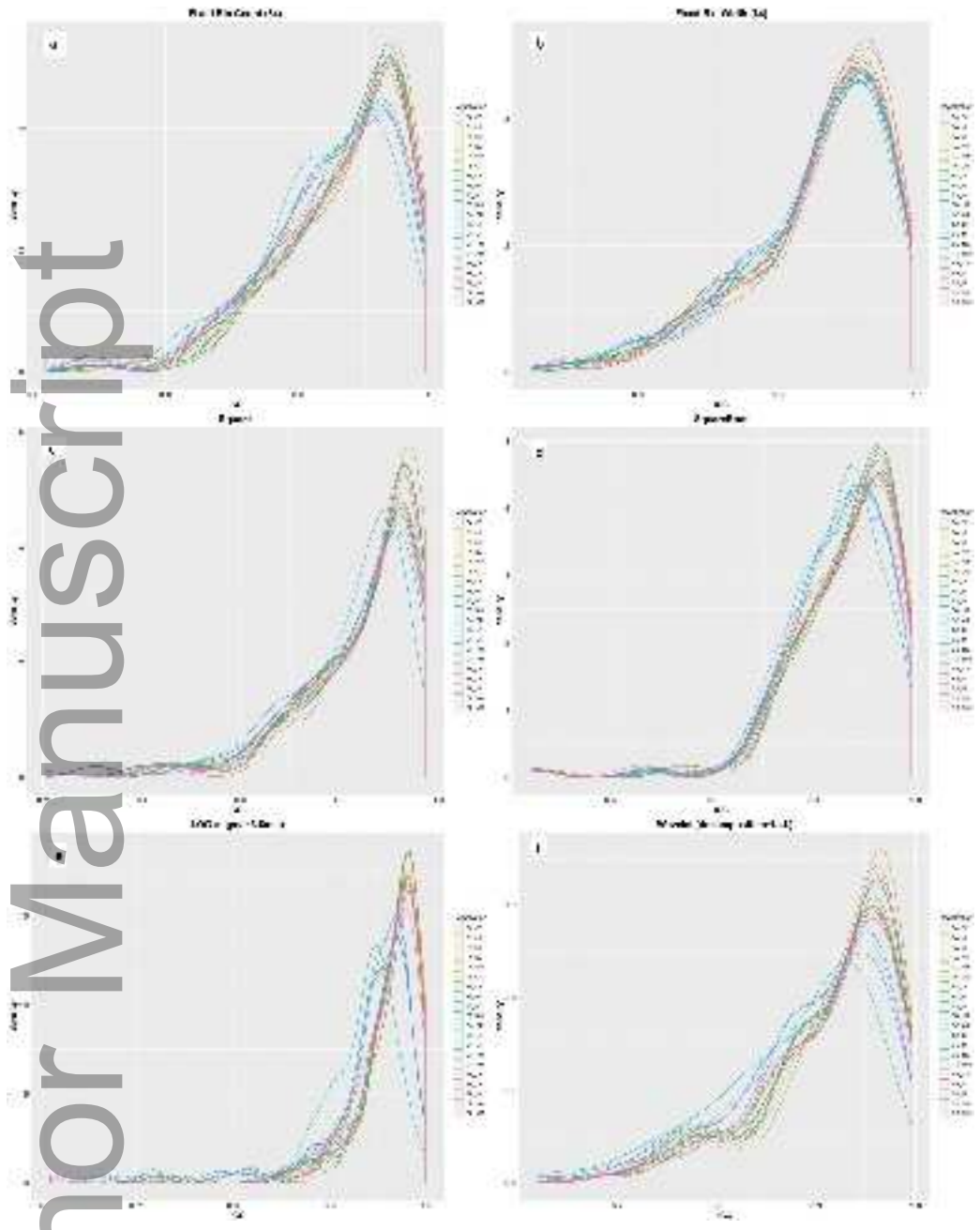


mp_14368_f5.jpg



mp_14368_f6.jpg

Author Manuscript



mp_14368_f7.jpg